Complex transitions between spike, burst or chaos synchronization states in coupled neurons with coexisting bursting patterns*

Gu Hua-Guang(古华光)[a)†], Chen Sheng-Gen(陈胜根)[a)], and Li Yu-Ye(李玉叶)[b)]

[a)] *School of Aerospace Engineering and Applied Mechanic, Tongji University, Shanghai* 200092, *China*
[b)] *Mathematics & Statistics Institute, Chifeng University, Chifeng* 024000, *China*

(Received 2 September 2014; revised manuscript received 15 October 2014; published online 27 March 2015)

We investigated the synchronization dynamics of a coupled neuronal system composed of two identical Chay model neurons. The Chay model showed coexisting period-1 and period-2 bursting patterns as a parameter and initial values are varied. We simulated multiple periodic and chaotic bursting patterns with non-(NS), burst phase (BS), spike phase (SS), complete (CS), and lag synchronization states. When the coexisting behavior is near period-2 bursting, the transitions of synchronization states of the coupled system follows very complex transitions that begins with transitions between BS and SS, moves to transitions between CS and SS, and to CS. Most initial values lead to the CS state of period-2 bursting while only a few lead to the CS state of period-1 bursting. When the coexisting behavior is near period-1 bursting, the transitions begin with NS, move to transitions between SS and BS, to transitions between SS and CS, and then to CS. Most initial values lead to the CS state of period-1 bursting but a few lead to the CS state of period-2 bursting. The BS was identified as chaos synchronization. The patterns for NS and transitions between BS and SS are insensitive to initial values. The patterns for transitions between CS and SS and the CS state are sensitive to them. The number of spikes per burst of non-CS bursting increases with increasing coupling strength. These results not only reveal the initial value- and parameter-dependent synchronization transitions of coupled systems with coexisting behaviors, but also facilitate interpretation of various bursting patterns and synchronization transitions generated in the nervous system with weak coupling strength.

Keywords: synchronization transition, phase synchronization, coexisting attractors, coupled neuronal system

PACS: 05.45.Xt, 87.18.Tt, 87.18.Hf **DOI:** 10.1088/1674-1056/24/5/050505

1. Introduction

Synchronization is widespread in nature.[1,2] Chaos synchronization has been one of the most important issues.[1,3] In particular, synchronization was experimentally detected in the nervous system of the mammalian visual cortex, the human thalamocortical area, and the stomatogastric ganglion of the spiny lobster.[4–6] Transitions between various synchronization states were observed in the oddball task experiment and evidenced in the human cardiorespiratory system.[7–9] It is believed that synchronization and synchronization transition are closely related to nervous information transmission and processing.[4,8–11] Physiologically, bursting is an important neural rhythm in the nervous system and is also important for information processing.[12–16] Recently, there have been various simulations of synchronization and synchronization transition in the nervous system.[17–22]

In most investigations of synchronization, the unit in the network or coupled system always manifests mono-stable behaviors. With the exception of mono-stable behavior, multi-stable and/or coexisting states are also common behaviors of a nonlinear system. The coexisting behavior of the dynamic system for a given set of parameters is determined by the initial values. Multi-stable behaviors occur in multiple fields, including biological science.[23] In the nervous system, the coexistence of resting condition and firing,[24–26] of spiking and bursting,[27–29] and of two different bursting patterns[30] were observed in experiments and simulated in theoretical models.

Recently, a few works have focused on the synchronization of unidirectionally coupled systems,[31–38] which manifest, when isolated, multi-stable or coexisting behaviors. These studies are briefly described as follows. Two coupled Rössler-like electronic circuits with coexisting chaotic attractors were investigated experimentally and numerically.[31–33] In that work the synchronization transitions moves from asynchronous motion to intermittent anticipating phase synchronization and generalized synchronization moves to a completely synchronized state as the coupling strength increases. The behaviors of asynchronous synchronization jump between the coexisting attractors. The synchronization dynamics of two coupled bistable Hénon maps were investigated.[34] When two periodic orbits coexist, the slave map evolves into the master map state. When chaotic and periodic attractors coexist, very complex dynamics, such as the emergence of new attractors are observed. Synchronization of coupled optical bistable systems with coexisting different attractors (fixed point and chaos, fixed point and one periodic orbit, and two periodic or-

*Project supported by the National Natural Science Foundation of China (Grant Nos. 11372224 and 11402039) and the Fundamental Research Funds for Central Universities designated to Tongji University (Grant No. 1330219127).

†Corresponding author. E-mail: guhuaguang@tongji.edu.cn

© 2015 Chinese Physical Society and IOP Publishing Ltd

bits) was investigated.[35]

Depending on both the control parameters of an isolated system and the coupling strength, different bifurcations and diverse dynamic regimes including periodicity and chaos occur in the route from asynchronous motion to complete synchronization. There also exists work on the nervous systems with bi-directional coupling.[36,37] One previous study[36] investigates the synchronization transitions of two coupled neurons with coexisting spiking and bursting. Three different configurations of a coupled system, one neuron spiking and the other bursting, both types of spikings and both types of burstings, are considered. The complete synchronization at stronger coupling strength and synchronization transitions depends on the configurations. For the configuration of one spiking and the other bursting, the synchronization transitions for three parameter values within the coexisting parameter region was investigated.[37] The results showed that the complete synchronization and synchronization transition depend on the parameter values. In both investigations, only one initial value is considered, and the influences of different initial values on the complete synchronization and synchronization transitions have not been addressed.

In this paper, we comprehensively study the synchronization and synchronization transitions of two bi-directionally coupled Chay model neurons with coexisting burstings. We considered different configurations of the network, the initial values and the control parameters. We investigated different synchronization states, various bursting patterns corresponding to different synchronization states, and complex synchronization transitions, which range from non-synchronization to complete synchronization and is composed of different synchronization states. We identified the dependence of the complete synchronization on the initial values and control parameters. We also identified the synchronization transitions containing transitions between spike and burst phase synchronization (i.e., chaos synchronization), and transitions between spike and complete synchronization. The rest of this paper is organized as follows. Section 2 describes the Chay model and the coexisting burstings. Section 3 introduces the network model, initial values, and criteria for synchronization. The synchronization states and the corresponding rhythms are introduced in Section 4. Section 5 provides the detailed synchronization transitions and the influence of the parameter and initial values. Section 6 is the conclusion and discussion.

2. Chay model and dynamics of single neuron

2.1. Chay model

The Chay model was initially set up to describe the bursting patterns of β-cells[39] and manifested bifurcations similar to those observed in an experimental neural pacemaker.[40–42] The Chay model is described using the following three differential equations:

$$\frac{\mathrm{d}V}{\mathrm{d}t} = g_i m_\infty^3 h_\infty (V_i - V) + g_{kv}(V_k - V)n^4 + g_{kc}\frac{C}{1+C}(V_k - V) + g_l(V_l - V), \quad (1)$$

$$\frac{\mathrm{d}n}{\mathrm{d}t} = \frac{n_\infty - n}{\tau_n}, \quad (2)$$

$$\frac{\mathrm{d}C}{\mathrm{d}t} = \rho(m_\infty^3 h_\infty (V_\mathrm{C} - V) - K_\mathrm{C} C). \quad (3)$$

Here, V, n, and C are the membrane potential, the probability of opening the voltage-sensitive K^+ channel, and the intracellular concentration of Ca^{2+}, respectively. V_i, V_k, and V_l are the reversal potentials for mixed Na^+–Ca^{2+}, K^+, and leakage ions, respectively. g_i, g_{kv}, g_{kc}, and g_l represent the maximum conductance of the mixed Na^+–Ca^{2+}, voltage-dependent K^+, calcium-dependent potassium, and leakage ions, respectively. m_∞ and h_∞ are the probabilities of activation and inactivation of the mixed inward current channel, and n_∞ is the steady state value of n. m_∞, h_∞, and n_∞ could be expressed by $y_\infty = \alpha_y/(\alpha_y + \beta_y)$ in general, y stands for m, h, or n, and $\alpha_m = 0.1(25+V)/(1-\mathrm{e}^{-0.1V-2.5})$, $\beta_m = 4\,\mathrm{e}^{-(V+50)/18}$, $\alpha_\mathrm{h} = 0.07\,\mathrm{e}^{-0.05V-2.5}$, $\beta_\mathrm{h} = 1/(1+\mathrm{e}^{-0.1V-2})$, $\alpha_n = 0.01(20+V)/(1-\mathrm{e}^{-0.1V-2})$, $\beta_n = 0.125\,\mathrm{e}^{-(V+30)/80}$. The relaxation time of the voltage-gated K^+ channel is $\tau_n = 1/(\lambda_n(\alpha_n+\beta_n))$. K_C is the rate constant for the efflux of the intracellular Ca^{2+} ions, and ρ is a proportionality constant. The parameter values of the Chay model are as follows: $g_i = 1800$, $g_{kv} = 1700$, $g_{kc} = 10$, $g_l = 7$, $V_k = -75$, $V_l = -40$, $V_i = 100$, $K_\mathrm{c} = 3.3/18$, $\lambda_n = 227.5$, $\rho = 0.27$. The unit of potential, conductance, and time is mV, pS, and sec, respectively. Detailed descriptions of the Chay model are given in a previous study.[39]

The parameter V_C, the reversal potential of Ca^{2+}, here serves as the bifurcation parameter. The Chay model is solved using the fourth-order Runge–Kutta integration method with time step of 0.001 sec.

2.2. Coexistence of period-1 bursting and period-2 bursting

When $V_\mathrm{C} = 308.1$, the coexistence of period-1 bursting and period-2 bursting can be simulated with the Chay model. When the initial values of (V, n, C) are set to (−47.733563, 0.105692, 0.511172) for period-1 bursting and (−48.365978, 0.100857, 0.518610) for period-2 bursting, the Chay model exhibits period-1 bursting (Fig. 1(a)) and period-2 bursting (Fig. 1(b)), respectively. The inter-spike interval (ISI) of period-1 bursting is a constant value, and the period-2 bursting exhibits two different ISIs.

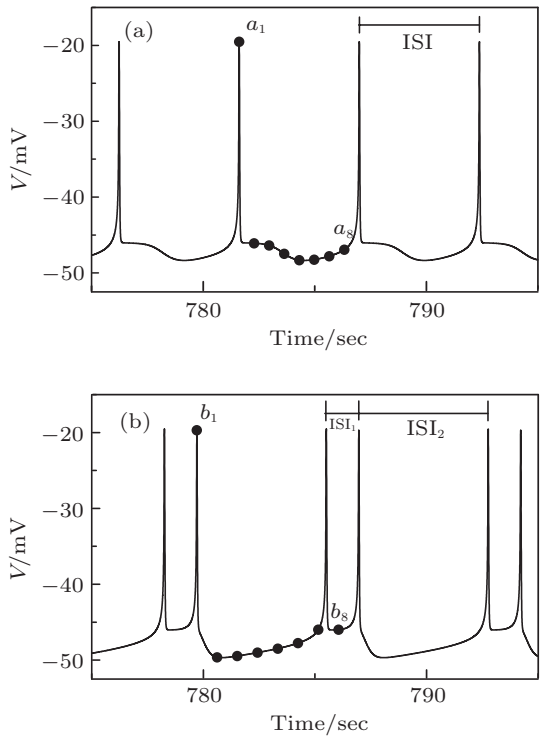


Fig. 1. Spike trains of the coexisting bursting of the Chay model when $V_C = 308.1$. (a) Period-1 bursting; eight dots labeled by a_i ($i = 1, 2, \ldots, 8$) are initial values of period-1 bursting. (b) Period-2 bursting; eight dots labeled by b_i ($i = 1, 2, \ldots, 8$) are initial values of period-2 bursting.

Bifurcation of ISI with respect to V_C is shown in Fig. 2. As V_C increases, period-2 bursting transforms to period-1 bursting at $V_C = 309.78$. As V_C decreases, period-1 bursting transforms to period-2 bursting at $V_C = 307.95$. $V_C \in [307.95, 309.78]$ is the region where period-1 and period-2 bursting coexist. When V_C is within this range, the Chay model exhibits either period-1 bursting or period-2 bursting; the choice depends on the initial values of (V, n, C). When $V_C > 309.78$, the behavior is mono-stable period-1 bursting. When $V_C < 307.95$, the behavior is mono-stable period-2 bursting.

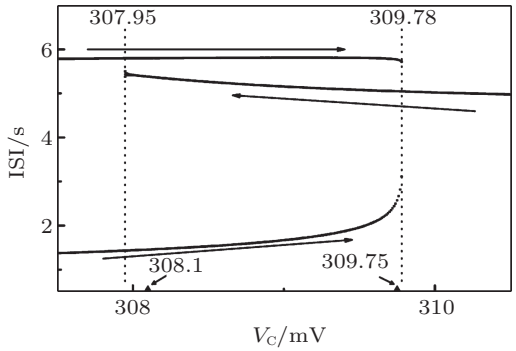


Fig. 2. Bifurcation of ISIs with respect to V_C of the Chay model.

2.3. The attraction domain

Because the attraction domain in the three-dimensional space (V, n, C) is difficult to visualize, we use the attraction domain in a two-dimensional cross-section (V, C) at a fixed n value which is easier to view. As shown in Figs. 3(a)–3(c), when $V_C = 308.1$, the attraction domain of period-1 bursting (black) and of period-2 bursting (white) in the (V, C) plane, corresponds to $n = 0.25$, 0.15, 0.3, respectively. The attraction domains in the (V, C) plane corresponding to $n = 0.25$, 0.15, 0.3, when $V_C = 309.75$ are shown in Fig. 3(d)–3(e), respectively. The ranges of V and C in Fig. 3(a) and Fig. 3(d) are much larger than in the other four figures. The ranges of V and C of Figs. 3(b)–3(c) and Figs. 3(e)–3(f) nearly equal those of the stable period-1 and period-2 bursting patterns. As can be seen from Fig. 3, as V_C increases, the black area increases while the

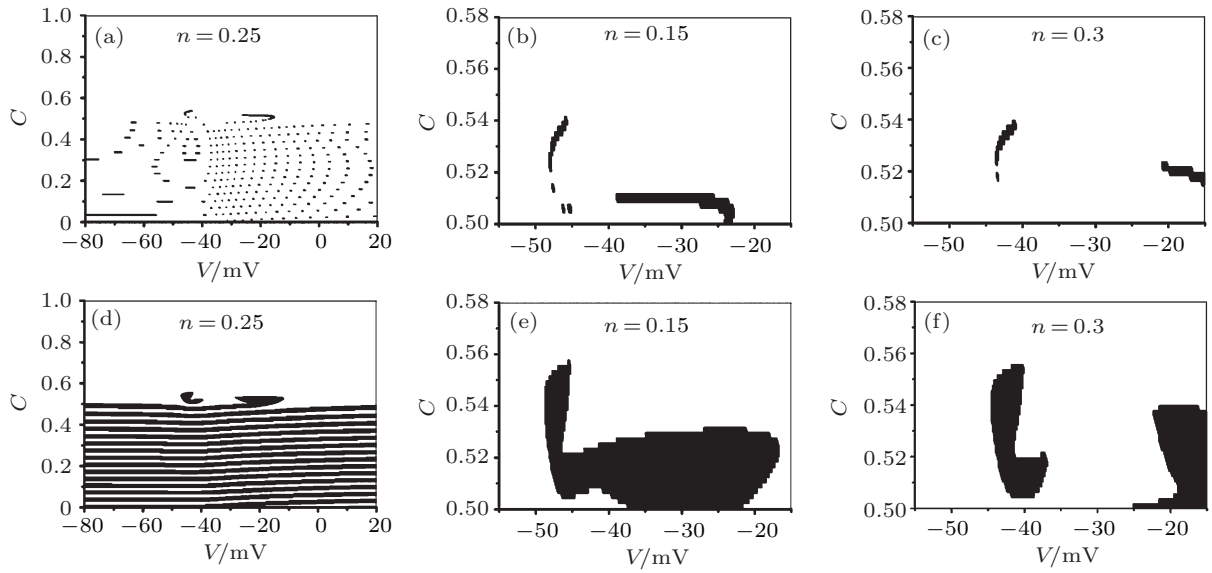


Fig. 3. The two-dimensional cross-section in the (V, C) plane of three-dimensional attraction domain of the coexisting period-1 bursting (black) and period-2 bursting (white) at different n value with different V_C. $V_C = 308.1$: (a) $n = 0.25$; (b) $n = 0.15$; (c) $n = 0.3$. $V_C = 309.75$: (d) $n = 0.25$; (e) $n = 0.15$; (f) $n = 0.3$.

white area decreases, thus showing that the attraction domain of period-1 bursting increases while that of period-2 bursting decreases.

3. Coupled neuronal model and criteria for synchronization

3.1. Coupled neuronal model

The coupled system is constructed by two bi-directionally coupled identical Chay neurons with a gap junction,[43] which is an important coupling manner that encourages synchrony.[44] The equations of the coupled system are as follows:

$$\begin{aligned}\frac{dV_1}{dt} &= g_i m_\infty^3 h_\infty (V_i - V_1) + g_{kv}(V_k - V_1)n_1^4 \\ &\quad + g_{kc}\frac{C_1}{1+C_1}(V_k - V_1) + g_l(V_l - V_1) \\ &\quad + g_c(V_2 - V_1), \qquad (4)\\ \frac{dn_1}{dt} &= \frac{n_\infty - n_1}{\tau_n}, \qquad (5)\\ \frac{dC_1}{dt} &= \rho(m_\infty^3 h_\infty (V_C - V_1) - K_C C_1), \qquad (6)\\ \frac{dV_2}{dt} &= g_i m_\infty^3 h_\infty (V_i - V_2) + g_{kv}(V_k - V_2)n_2^4 \\ &\quad + g_{kc}\frac{C_2}{1+C_2}(V_k - V_2) + g_l(V_l - V_2) \\ &\quad + g_c(V_1 - V_2), \qquad (7)\\ \frac{dn_2}{dt} &= \frac{n_\infty - n_2}{\tau_n}, \qquad (8)\\ \frac{dC_2}{dt} &= \rho(m_\infty^3 h_\infty (V_C - V_2) - K_C C_2). \qquad (9)\end{aligned}$$

Here, the subscripts 1 and 2 indicate neurons 1 and 2, respectively. The parameter g_c is the coupling strength. It varies from 0 to 35 in steps of 0.01. The values of other parameters are the same as those of a single neuron. The coupling item of neuron 1 is $g_c(V_2 - V_1)$. The equations are solved numerically using the fourth-order Runge–Kutta integration method with integration time step of 0.001 sec.

3.2. Values of parameter V_C

Two values of V_C within the coexistence region are chosen, indicated by two arrows in Fig. 2. One is 308.1 mV, which is close to the mono-stable period-2 bursting. The other is 309.75 mV, which is close to the mono-stable period-1 bursting.

3.3. Initial values

When $V_C = 308.1$, eight initial values with equal intervals spanning both period-1 bursting and period-2 bursting, as indicated by dots in Figs. 1(a) and 1(b), are numbered as a_i and b_i ($i = 1,2,\ldots,8$), respectively, from left to right. For the configuration when one neuron has period-1 bursting and the other period-2 bursting, the 64 initial values $a_i b_j$ ($i = 1,2,\ldots,8; j = 1,2,\ldots,8$) are different. For the configuration when both neurons show period-1 bursting, one can ignore the case of $i = j$ ($i = 1,2,\ldots,8$) that lead to coupling-independent compete synchronization and the case of symmetry of i and j; then there are $(64-8)/2 = 28$ different initial values $a_i a_j$ ($i = 1,2,\ldots,7; j = i+1,\ldots,8$). Similarly, there are 28 different $b_i b_j$ ($i = 1,2,\ldots,7; j = i+1,\ldots,8$) values for configuration of when both neurons show period-2 bursting. Thus, a total of 120 (64 + 28 + 28) different initial values are used for $V_C = 308.1$.

Similarly, 120 different initial values are also used for $V_C = 309.75$.

3.4. Criteria for synchronization

We investigate complete synchronization and phase synchronization. Both spike and burst phase synchronizations are considered. The spike phase function ($\phi_l(t)$) of the firing pattern of neuron l ($l = 1,2$) can be defined as follows:

$$\begin{aligned}&\phi_l(t) = 2k\pi + 2\pi\frac{t - t_k^l}{t_{k+1}^l - t_k^l},\\ &(t_k^l \le t < t_{k+1}^l),\ \ k_l = 1,2,...,N. \qquad (10)\end{aligned}$$

Here, t_k^l is the time of the k^{th} spike of neuron l (l = 1, 2), and N is the number of spikes. The spike phase difference ($\Delta\phi(t)$) between two coupled neurons is defined as $\Delta\phi(t) = |\phi_1(t) - \phi_2(t)|$. Different spike phase synchronization states can be distinguished by the maximum value of $\Delta\phi(t)$, labeled as $\max(\Delta\phi(t))$, shown as follows:

(i) The complete synchronization (CS) state when $\max(\Delta\phi(t)) = 0$.

(ii) The spike phase synchronization (SS) state when $0 < \max(\Delta\phi(t)) \le 2\pi$.

(iii) Non-spike phase synchronization state when $\max(\Delta\phi(t)) > 2\pi$.

When the behavior of the two coupled neurons exhibits non-spike phase synchronization, the burst spike synchronization is considered. The burst phase function ($\Phi_l(t)$) of firing pattern of neuron l ($l = 1,2$) can be defined as follows:

$$\begin{aligned}&\Phi_l(t) = 2k\pi + 2\pi\frac{t - T_k^l}{T_{k+1}^l - T_k^l},\\ &(T_k^l \le t < T_{k+1}^l),\ \ k_l = 1,2,...,M. \qquad (11)\end{aligned}$$

Here, T_k^l is the time of the first spike of the k^{th} burst of neuron l ($l = 1,2$), and M is the number of the bursts. The burst phase difference between two coupled neurons is defined as $\Delta\Phi(t) = |\Phi_1(t) - \Phi_2(t)|$. Burst phase synchronization is characterized by the maximum value of $\Delta\Phi(t)$ labeled $\max(\Delta\Phi(t))$ as follows:

(1) Burst phase synchronization (BS) state when $0 < \max(\Delta\Phi(t)) \le 2\pi$.

(2) Non-burst phase synchronization (NS) state when $\max(\Delta\Phi(t)) > 2\pi$.

In addition, lag synchronization (LS) is also considered for some firing patterns. Spike trains of neuron 1 and neuron 2 overlap for LS of firing patterns if one neuron moves forward or backward along time axis and the other remains fixed.

4. Synchronization states and the firing patterns

4.1. Complete synchronization (CS)

CS of period-1 bursting and period-2 bursting can be simulated, as shown in Fig. 4. For example, spike trains of period-1 bursting of CS are shown in the upper two rows of Fig. 4(a) for the conditions when $V_C = 309.75$, initial value b_5b_6, and $g_c = 5.0$. The spike trains of period-2 bursting of CS are shown in the upper two rows of Fig. 4(b) for the conditions when $V_C = 308.1$, a_1b_2, and $g_c = 4.0$. The spike phase differences of both bursting patterns equal zero, as shown in the bottom row of Figs. 4(a) and 4(b).

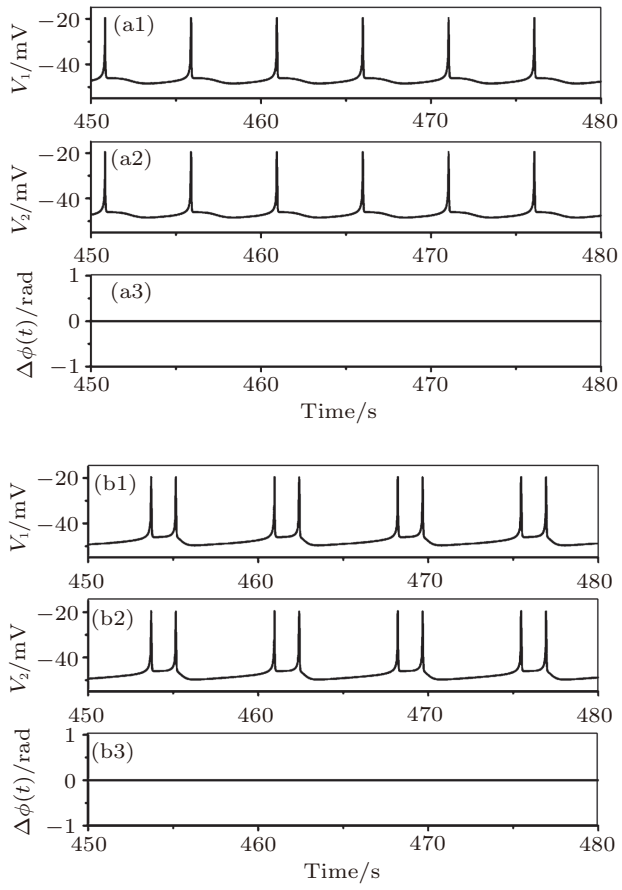


Fig. 4. The complete synchronization. (a) Period-1 bursting; (b) period-2 bursting. From top to bottom: spike train of neuron 1, spike train of neuron 2, and spike phase difference ($\Delta\phi(t)$) between neurons 1 and 2.

4.2. Spike phase synchronization (SS)

Spike phase synchronization (SS) can be simulated and the corresponding firing patterns include various periodic and chaotic bursting patterns.

4.2.1. Periodic bursting patterns

A period-3 bursting ($V_C = 308.1$, initial value a_1b_2, and $g_c = 1.08$) is shown in Fig. 5(a), containing one burst per period and three spikes per burst. A period-(3,3) bursting ($V_C = 308.1$, initial value a_1b_2, and $g_c = 1.3$) is illustrated in Fig. 5(b), composed of two bursts per period and three spikes in the both bursts. The ISIs of the three spikes in the first burst are different from those of the second. A period-(7,8) bursting ($V_C = 308.1$, initial value a_1b_2, and $g_c = 3.3$) is shown in Fig. 5(c), containing two bursts per period. One burst contains seven spikes and the other eight spikes. In addition, period-k ($k = 2,4$) bursting, period-(k, k) ($k = 2,4,5,6$) bursting and period-(k, $k+1$) ($k = 2,3,4,5,6$) bursting are simulated.

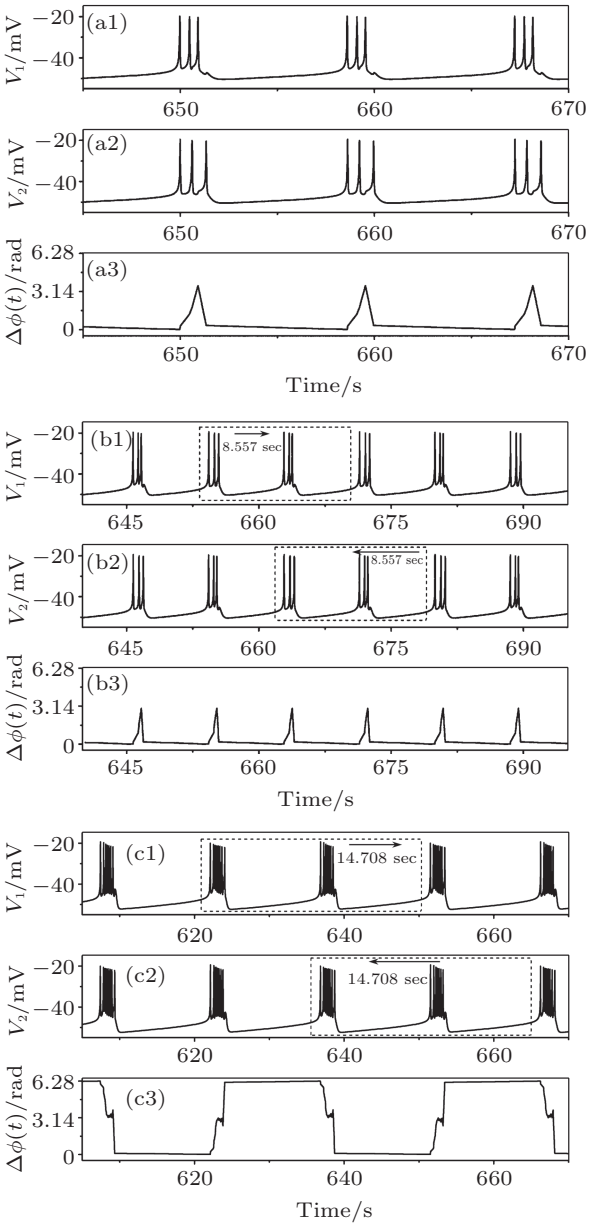


Fig. 5. Spike phase synchronization of periodic bursting. (a) Period-3 bursting; (b) period-(3, 3) bursting; (c) period-(7, 8) bursting. From top to bottom: spike train of neuron 1, spike train of neuron 2, and spike phase difference between neurons 1 and 2.

For the period-k ($k = 2,3,4$) bursting and period-(k, k) ($k = 2,3,4,5,6$) bursting, spikes in the two firing trains within the same time duration exhibit one-to-one correspondence, so $\max(\Delta\phi(t))$ is less than 2π, as shown in the lowest row of Figs. 5(a) and 5(b). For period-(k, $k+1$) bursting ($k = 2,3,4,5,6$), the burst with k spikes of one neuron corresponds to the burst with $k+1$ spikes of the other neuron. The $\max(\Delta\phi(t))$ almost approaches but remains below 2π (bottom row of Fig. 5(c)). All of the above results show that the periodic bursting events are in the SS state.

4.2.2. Chaotic bursting patterns

Chaotic bursting patterns include chaos-2 bursting and chaos-(1, 2) bursting. Chaos-2 bursting is composed of bursts with two spikes. Chaos-(1, 2) bursting is composed of bursts containing one spike or two spikes. An example of chaos-2 bursting ($V_C = 308.1$, initial value a_1b_2, and $g_c = 0.45$), and an example of chaos-(1, 2) ($V_C = 309.75$, initial value a_5a_7, and $g_c = 0.01$) are shown in Figs. 6(a) and 6(b), respectively. The largest Lyapunov exponents (LEs) of the two firing patterns are 0.58 and 0.26 greater than 0, respectively. The chaos-(1, 2) bursting manifests behaviors that jump between the two coexisting attractors, which is similar to the behaviors that jump between two coexisting chaotic attractors in a previous study.

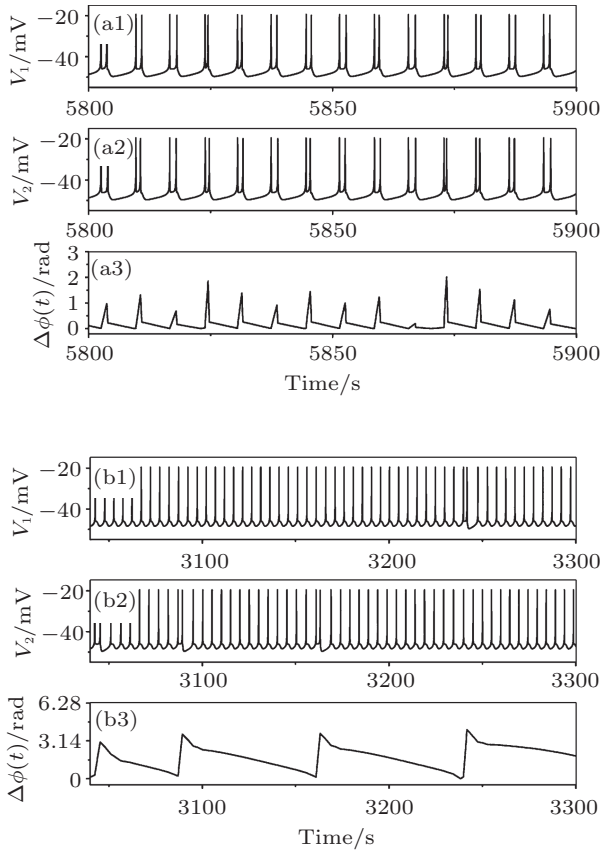


Fig. 6. Spike phase synchronization of chaotic bursting. (a) Chaos-2 bursting; (b) chaos-(1, 2) bursting. From top to bottom: spike train of neuron 1, spike train of neuron 2, and spike phase difference between neurons 1 and 2.

For the chaos-2 bursting, the $\max(\Delta\phi(t))$ is bounded within 2π due to one-to-one correspondence between spikes from the two neurons. For the chaos-(1, 2) bursting, bursts with one spike appear continuously and are interrupted by single bursts with two spikes. Bursts with two spikes do not appear continuously. The $\max(\Delta\phi(t))$ is less than 2π.

4.3. Burst phase synchronization (BS)

Bursting patterns of BS include three types: another kind of chaos-(1, 2) bursting, chaos-(2, 3) bursting composed of bursts with 2 and 3 spikes, and chaos-(2, k, $k+1$) ($k = 3,4$) bursting composed of bursts with 2, k, and $k+1$ spikes. A chaos-(1, 2) bursting ($V_C = 309.75$, initial value a_5a_7, and $g_c = 0.11$), a chaos-(2, 3) bursting ($V_C = 308.1$, initial value a_1b_2, and $g_c = 0.82$), and a chaos-(2, 3, 4) bursting ($V_C = 308.1$, initial value a_1b_2, and $g_c = 1.70$) are shown in Figs. 7(a)–7(c), respectively.

The three firing patterns show non-spike synchronization, as shown by the third row of Figs. 7(a)–7(c). As can be seen from the second burst to the fourth burst of Fig. 7(a), three spikes appear in neuron 1 and five spikes appear in neuron 2. A procedure changing from uncoupling to coupling of the behaviors of the two neurons is shown in Fig. 7(b). Neurons 1 and 2, when isolated (before $t = 0$ s), exhibit period-1 bursting and period-2 bursting, respectively. The two neurons are coupled together at $t = 0$ s. Then, two coupled neurons immediately exhibit non-spike phase synchronization but burst phase synchronization of bursting pattern with two or three spikes. Some bursts with two spikes of one neuron may correspond to the bursts with three spikes of the other neuron. For example, there are three spikes in the first and fourth bursts of neuron 1 while there are two spikes in the two bursts of neuron 2. The spike phase difference exceeds 2π. The evolvement of chaos-(2,3,4) and changes of phase difference with varying time are illustrated in Fig. 7(c). Different from Fig. 7(b), the spike phase synchronization lasts about 180 s before changing to non-spike synchronization but burst synchronization. Within the 180 s, the spike phase difference less than π lasts about 150 s at first, and then changed to a value between π and 2π.

For the three chaotic firing patterns, bursts from two firing trains within the same time span exhibit a one-to-one correspondence, so the $\max(\Delta\Phi(t))$ is less than 2π, as shown in the lowest row of Figs. 7(a)–7(c).

4.4. Non-burst phase synchronization (NS)

A chaos-(1, 2) bursting when $V_C = 309.75$, initial value a_3b_1, and $g_c = 0.08$ is shown in Fig. 8. When time falls between 2410 and 2480 s (Fig. 8(a)), the number of spikes of neuron 1 is 18, while that of neuron 2 is 15. When time falls between 2017 and 2120 s (Fig. 8(b)), there are 17 bursts for neuron 1 and 19 bursts for neuron 2. Both $\Delta\phi(t)$ and $\Delta\Phi(t)$

are larger than 2π, showing that the bursting pattern is non-spike or non-burst phase synchronization.

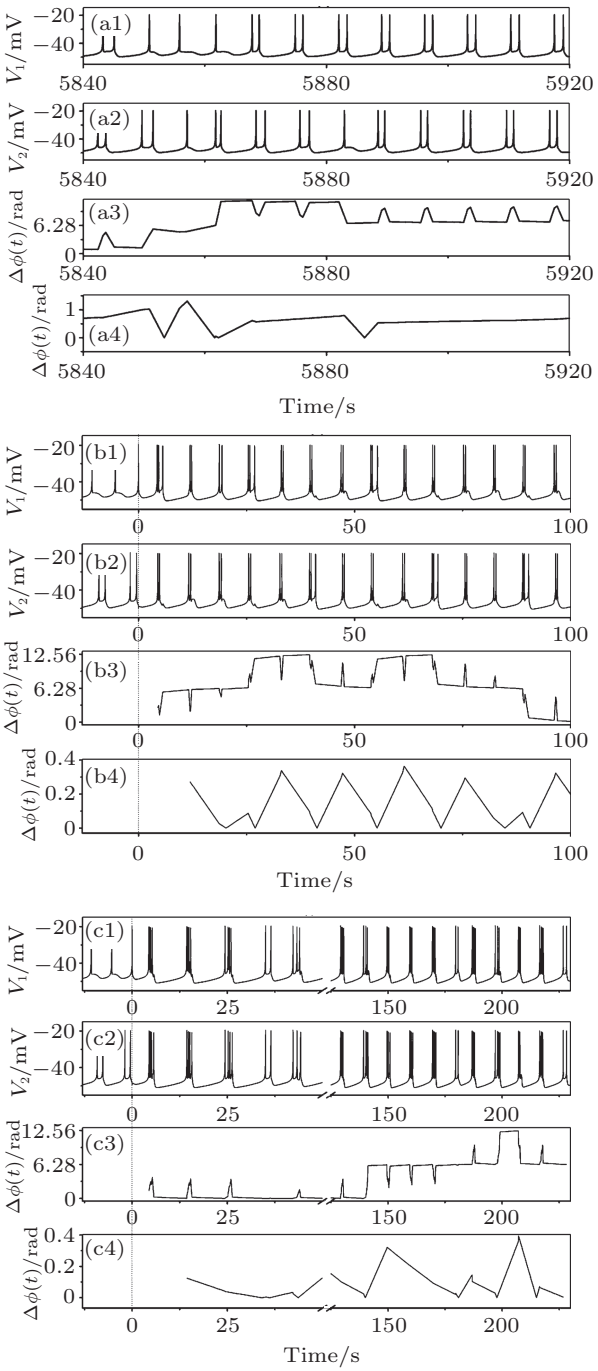


Fig. 7. Burst phase synchronization. (a) Chaos-(1, 2) bursting; (b) from burstings of two isolated uncoupling neurons to chaos-(2, 3) bursting of coupled neurons; (c) from burstings of two isolated uncoupling neurons to chaos-(2, 3, 4) bursting of coupled neurons. Dashed lines in (b) and (c) represent the time of coupling strength changed from 0 to a nonzero value. From top to bottom: spike train of neuron 1, spike train of neuron 2, spike phase difference ($\Delta\phi(t)$), and burst phase difference ($\Delta\Phi(t)$).

4.5. Lag synchronization (LS)

Period-(k, k) ($k = 2,3,4,5,6$) and period-(k, $k+1$) ($k = 2,3,4,5,6,7$) bursting with spike phase synchronization are also identified as lag synchronization. For instance, the spike trains of neuron 1 and neuron 2 can overlap if one of the spike trains is moved along the time axis and the other is fixed, as shown by the dashed boxes and arrows in Figs. 5(b) and 5(c). The time difference between two spike trains is also shown in the figures.

4.6. Summary of the synchronization states

Different synchronization states and the corresponding firing patterns are summarized in Table 1.

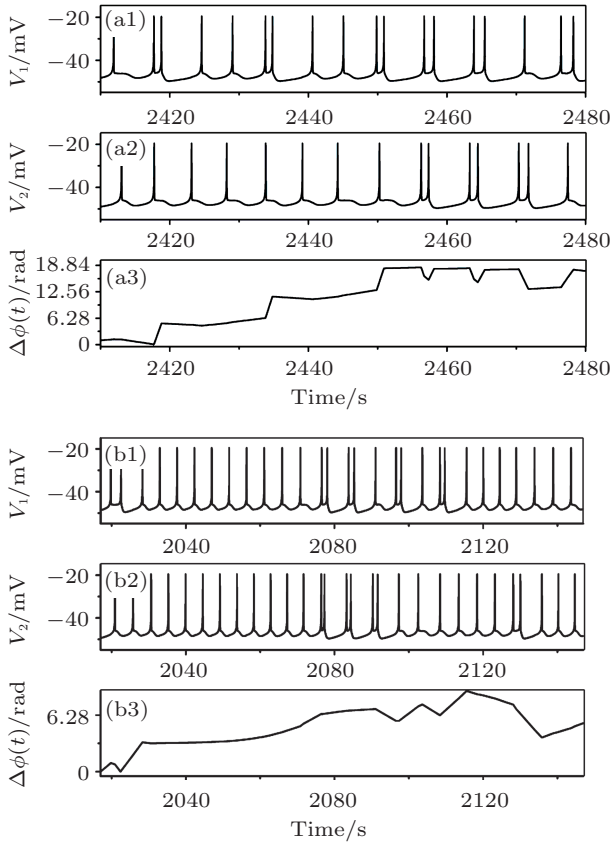


Fig. 8. Non-burst phase synchronization. Chaos-(2, 3) bursting when $V_C = 309.75$ mV, initial value a_3b_1, and $g_c = 0.08$; (a) Time is between 2410 sec and 2480 sec; upper: spike train of neuron 1; middle: spike train of neuron 2; lower: spike phase difference ($\Delta\phi(t)$); (b) time is between 2017 sec and 2047 sec; upper: spike train of neuron 1; middle: spike train of neuron 2; lower: burst phase difference ($\Delta\Phi(t)$).

Table 1. The correspondence between synchronization states and bursting patterns.

Synchronization state	Bursting pattern	Example
CS	Period-k (k = 1, 2)	Fig. 4
SS(LS)	Period-(k, k) (k = 2, 3, 4, 5, 6)	Fig. 5(b)
	Period-(k, k + 1) (k = 2, 3, 4, 5, 6, 7)	Fig. 5(c)
	Period-k (k = 2, 3, 4)	Fig. 5(a)
SS	Chaos-2	Fig. 6(a)
	Chaos-(1, 2) (g_c = 0.01, 0.02)	Fig. 6(b)
BS	Chaos-(1, 2) (g_c = 0.11)	Fig. 7(a)
	Chaos-(2, 3)	Fig. 7(b)
	Chaos-(2, k, k + 1) (k = 3, 4)	Fig. 7(c)
NS	Chaos-(1, 2) (g_c = 0.02, [0.04,0.10])	Fig. 8

5. Transitions between synchronization states

As g_c increases, the two coupled neurons achieve complete synchronization states via a complex processes composed of different synchronization states. For convenience, the transitions between synchronization states with increasing g_c is called a synchronization transition process in the present paper. The dependence of parameter V_C and the initial values on the transition processes are investigated. One hundred and twenty initial values are considered for both $V_C = 308.1$ and $V_C = 309.75$.

5.1. Synchronization transitions when $V_C = 308.1$

5.1.1. Basic structure of the transitions

The transitions with an initial value a_1b_2 is shown in Fig. 9. The ISIs of neurons 1 and 2 are shown in Figs. 9(a) and 9(b), respectively. According to the maximum values of spike and burst phase difference shown in Figs. 9(c) and 9(d), the transitions are divided into three parts, as labeled by vertical bold dashed lines. Part 1 exhibits transitions between SS and BS ($g_c < 2.19$). Part 2 manifests transitions between SS and CS ($g_c \in [2.19, 3.32]$). Part 3 is the CS state ($g_c > 3.32$).

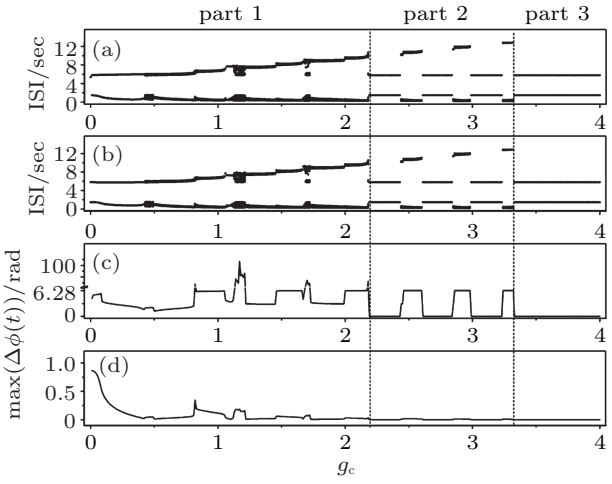


Fig. 9. Transitions with respect to g_c, when $V_C = 308.1$ and initial value a_1b_2. (a) ISIs of neuron 1; (b) ISIs of neuron 2; (c) maximum spike phase difference max($\Delta\phi(t)$); (d) maximum burst phase difference max($\Delta\Phi(t)$).

5.1.2. Part 1 of the synchronization transitions

Figure 10(a) is an enlargement of part 1 in Fig. 9(a). The SS and BS transit four times. The four SS states exist in ranges of $g_c \in [0.01, 0.81]$, [0.83, 1.11], [1.22, 1.67], and [1.73, 2.17], respectively, and the ranges of the four BS states are $g_c = 0.82$, [1.12, 1.21], [1.68, 1.72], and 2.18, respectively. According to the largest Lyaponov exponent (LE) shown in Fig. 10(b), the BS is identified as chaos synchronization and most of the SS is period synchronization with exception of the chaos-2 bursting at $g_c \in [0.43, 0.49]$. The transition between BS and SS is also the transition between chaos synchronization and period synchronization.

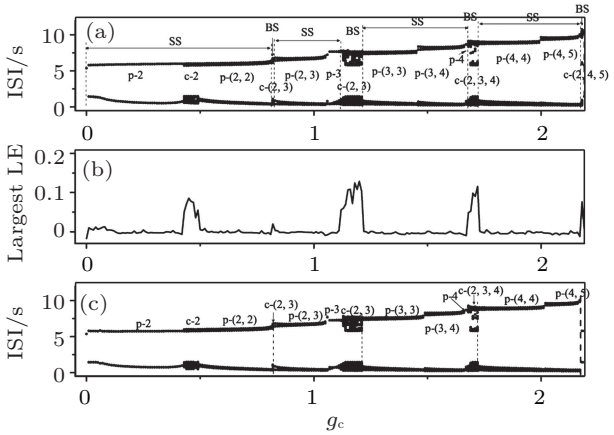


Fig. 10. Part 1 of the transitions of neuron 1 when $V_C = 308.1$. (a) The transitions with initial value a_1b_2; (b) the largest Lyapunov exponent correspond to the transitions with initial value a_1b_2; (c) the transitions with initial value a_7a_8. The characters "p" and "c" are abbreviations of "period" and "chaos," respectively.

As g_c increases, the bursting patterns appear in the following order: period-2, chaos-2, period-(2, 2), chaos-(2, 3), period-(2, 3), period-3, chaos-(2, 3), period-(3, 3), period-(3, 4), period-4, chaos-(2, 3, 4), period-(4, 4), period-(4, 5), and chaos-(2, 4, 5), as shown in Fig. 10(a). The largest number of spikes within a burst of bursting patterns of spike and burst synchronization increases with increasing g_c.

The detailed transitions of part 1 in Fig. 9 is not very sensitive to the initial values. The 120 transition processes corresponding to different initial values exhibit almost the same transition processes as shown in Fig. 10(a). For instance, a transition process with initial value a_7a_8, exhibit almost the same process as the one with initial value a_1b_2, as shown in Fig. 10(c). The difference between the two processes is described as follows. As shown in Fig. 10(a), the period-(3, 3) bursting appears when $g_c \in [1.22, 1.45]$ and period-(3, 4) appears when $g_c \in [1.46, 1.66]$; figure 10(c) shows that the period-(3, 3) bursting appears when $g_c \in [1.22, 1.48]$ and period-(3, 4) appears when $g_c \in [1.49, 1.66]$. The processes within the remaining ranges of g_c shown in Fig. 10(a) are the same as those shown in Fig. 10(c).

5.1.3. Part 2 of the synchronization transitions

Part 2 of the process shown in Fig. 9(a) is highlighted in Fig. 11(a). The right boundary is at $g_c = 3.32$. The transition between CS state and SS state happens three times. The ranges of the three CS states are $g_c \in [2.19, 2.43]$, [2.61, 2.84], and [2.99, 3.23] and of the three SS states are $g_c \in [2.44, 2.60]$, [2.85, 2.98], and [3.24, 3.32]. As g_c increases, ignoring the period-2 bursting of CS, the following types appear in order: period-(5,5), period-(5, 6), period-(6, 6), period-(6, 7), and period-(7, 8) bursting of SS. The period-(7, 8) bursting is the final bursting. This shows that the largest number of spikes within a bursting pattern of SS increases with increasing g_c.

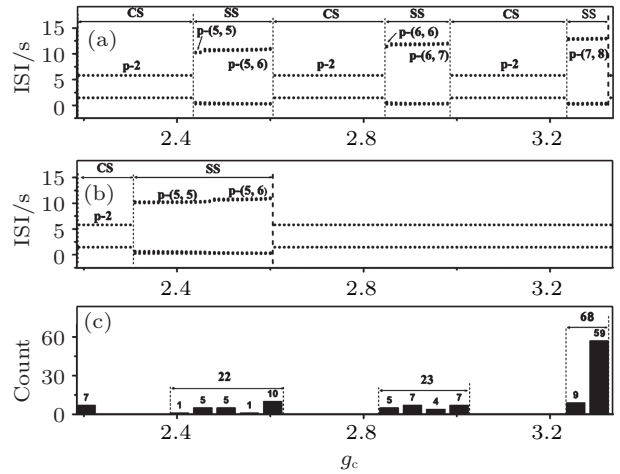


Fig. 11. Part 2 of the transitions of neuron 1 when $V_C = 308.1$. (a) The transitions with initial value a_1b_2; (b) the transitions with initial value a_7a_8; (c) dependence of the 120 initial values. The characters "p" and "c" are abbreviations of "period" and "chaos," respectively.

Part 2 of the process with initial values a_7b_8 is shown in Fig. 11(b). The right boundary is at $g_c = 2.60$. The transition between the CS state and SS state happens only once. The difference between these two transition processes with initial values a_1b_2 and a_7a_8 indicates that the detailed process is sensitive to initial values. The right boundary and times of transitions between SS and CS depend on the initial values.

Figure 11(c) illustrates the dependence of 120 initial values on the detailed processes. There are 68 processes that transit three times, and the right boundary of g_c is between 3.23 and 3.33. Twenty-three processes transit two times, and g_c of the right boundary is between 2.83 and 3.03. Twenty-two processes transits one time, and the g_c values of the right boundary are between 2.38 and 2.63. The remaining seven processes achieve the CS states of period-2 bursting that remains unchanged as g_c increases and do not experience transition.

5.1.4. Part 3 of the synchronization transitions

Part 3 of the process is in the CS state and is also sensitive to the initial values. The left boundary of g_c for part 3 depends on the right boundary of part 2. Out of the 120 processes 109 exhibit CS of period-2 bursting, which remains unchanged as g_c increases, as shown in Fig. 9(a); the remaining 11 processes manifest a transition from period-2 bursting to period-1 bursting of CS, which remains unchanged as g_c increases. This is shown in Fig. 12. Table 2 summarizes the details of how the bursting patterns of CS depend on the initial values. The results show that most initial values lead to period-2 bursting of CS, while only a few lead to period-1 bursting.

Table 2. The number of bursting patterns of complete synchronization when $V_C = 309.75$.

	Total number	Number of CS1	Number of CS2
Initial value a_ib_j	64	55	9
Initial value a_ia_j	28	21	7
Initial value b_ib_j	28	21	7
Sum	120	97	23

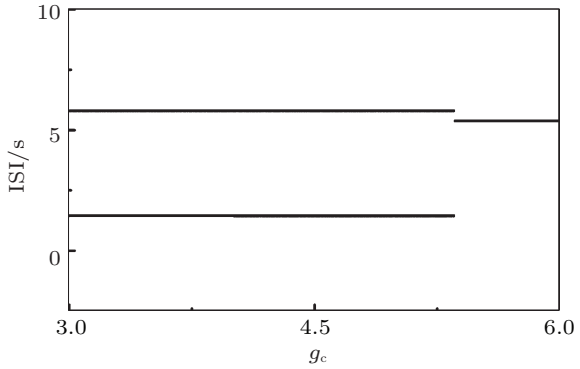


Fig. 12. Part 3 of the transitions when $V_C = 308.1$ and initial value a_8b_7.

5.2. Synchronization transitions when $V_C = 309.75$

5.2.1. Basic structure of transitions

A detailed transition processes with initial value b_5b_6 can be divided into four parts labeled by the bold vertical dashed lines in Fig. 13. Part 1 is almost in the non-burst synchronization (NS) state. Part 2 exhibits transitions between SS and BS states. Part 3 manifests transitions between SS and CS states. Part 4 is the CS state.

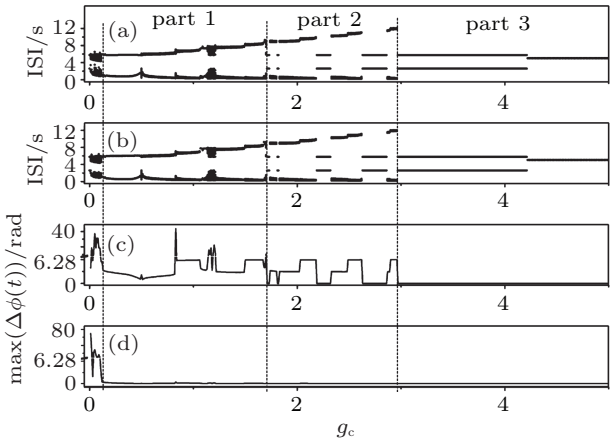


Fig. 13. Transitions with respect to g_c, when $V_C = 309.75$ and initial value b_5b_6. (a) ISIs of neuron 1; (b) ISIs of neuron 2; (c) maximum spike phase difference $\max(\Delta\phi(t))$; (d) maximum burst phase difference $\max(\Delta\Phi(t))$.

5.2.2. Part 1 of the synchronization transitions

Part 1 exhibits the NS state of chaos-(1, 2) bursting (Fig. 8) when $g_c < 0.12$, with three exceptions: $g_c = 0.01$, 0.03, and 0.11. When $g_c = 0.01$ and 0.03, the chaos-(1, 2) bursting is in the SS state (Fig. 6(b)). When $g_c = 0.11$, the chaos-(1,2) bursting exhibit BS (Fig. 7(a)). This part is insensitive to the initial value.

5.2.3. Part 2 of the synchronization transitions

Figures 14(a) and 14(b) are enlargement of part 2 from Fig. 13(a) as well as the largest Lyapunov exponent (LE) of

neuron 1. The transition between SS and BS states happen three times when $g_c \in [0.12, 1.70]$. These transitions also represent the transitions between chaos and period synchronizations. The ranges of the three SS states are $g_c \in [0.12, 0.82]$, $[0.84, 1.12]$, and $[1.22, 1.69]$, and those of the three BS states are $g_c = 0.83$, $[1.13, 1.21]$, and 1.70. As g_c increases, period-2, chaos-2, period-(2, 2), chaos-(2, 3), period-(2, 3), period-3, chaos-(2, 3), period-(3, 3), period-(3, 4), period-4, and chaos-(2, 3, 4) bursting appear in order.

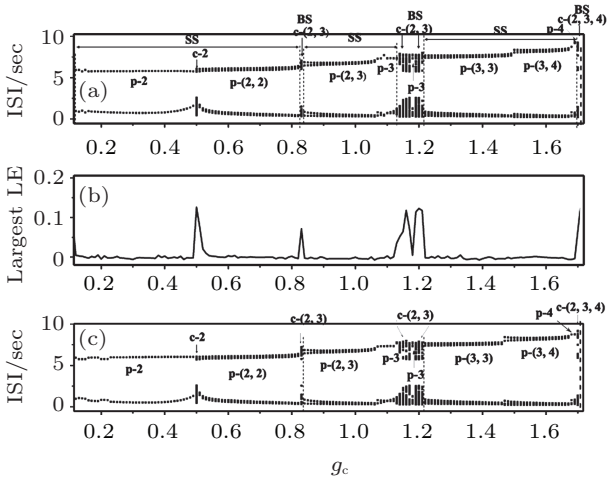


Fig. 14. Part 2 of the transitions of neuron 1 when $V_C = 309.75$. (a) The transitions with initial value b_5b_6; (b) the largest Lyapunov exponent correspond to the transitions with initial value b_5b_6; (c) the transitions with initial value a_3b_1. The characters "p" and "c" are abbreviations of "period" and "chaos," respectively.

The process with initial value a_3b_1 is shown Fig. 14(c). This exhibits almost the same process as that shown in Fig. 14(a), showing that the detailed process of part 2 is insensitive to the initial values. The small difference between the processes shown in Figs. 14(a) and 14(c) is not addressed in this paper. All 120 transition processes exhibit almost the same process.

5.2.4. Part 3 of the synchronization transitions

Part 3 of the process shown in Fig. 13(a) and that of neuron 1 with initial value a_3b_1 are shown in Figs. 15(a) and 15(b), respectively. The g_c values of right boundary and the times of transition between SS and CS are different. For example, the right boundary of Figs. 15(a) and 15(b) are $g_c = 2.96$ and $g_c = 3.30$, respectively.

Figure 15(c) shows how part 3 of the 120 processes depends on initial values. The g_c values of the right boundary of 70 processes are between 3.26 and 3.34, and transit 4 times between SS and CS. Seventeen processes transit three times, and g_c of the right boundary is between $g_c = 2.86$ and 3.01. Twenty-five processes transit two times, and the g_c value corresponding to the right boundary is between 2.26 and 2.63. Six processes transit one time, and g_c of the right boundary is between 1.89 and 2.19. The remaining two processes achieve the CS of period-2 bursting that remains unchanged as g_c increases and do not transit.

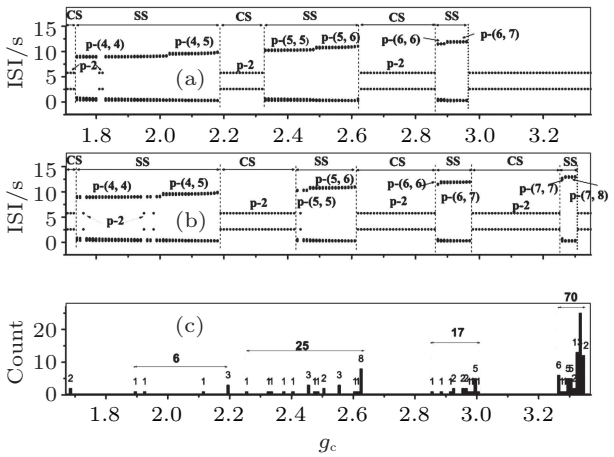


Fig. 15. Part 3 of the transitions of neuron 1 when $V_C = 309.75$. (a) The transitions with initial value b_5b_6; (b) the transitions with initial value a_3b_1; (c) dependence of the 120 initial values. The characters "p" and "c" are abbreviations of "period" and "chaos," respectively.

5.2.5. Part 4 of the synchronization transitions

Part 4 of the process is the CS state. This part is also sensitive to the initial value. Ninety-five out of the 120 process transit from period-2 bursting to period-1 bursting of CS, which remains unchanged as g_c increases. One example of this case is shown in Fig. 13(a). Two processes manifest the CS of period-1 bursting, which remains unchanged as g_c increases. The remaining 23 initial values lead to CS of period-2 bursting, which also remains unchanged as g_c increases, as shown in Fig. 16.

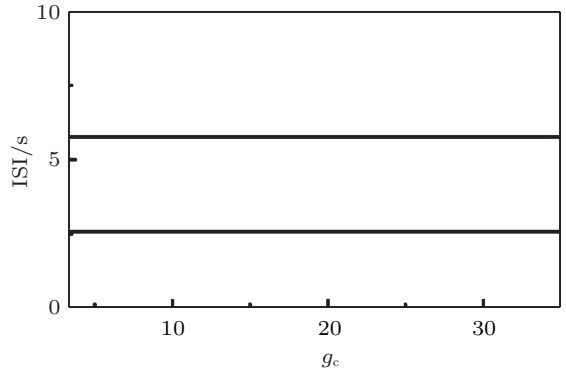


Fig. 16. Part 4 of the transitions when $V_C = 309.75$ and initial value a_3b_1.

The number of initial values that lead to unchanged period-1 bursting and period-2 bursting of CS is shown in Table 3. When $V_C = 309.75$, most initial values lead to period-1 bursting of CS, while only a few lead to period-2 bursting, which is just the opposite of the result when $V_C = 308.1$. This is consistent with attraction domains to a certain extend. When $V_C = 308.1$, the attraction domain of period-2 bursting is much

bigger than that of the period-1 bursting. When $V_C = 309.75$, the attraction domain of period-1 bursting increases.

Table 3. Number of bursting patterns of complete synchronization when $V_C = 308.1$.

	Total number	Number of CS1	Number of CS2
Initial value a_ib_j	64	5	59
Initial value a_ia_j	28	5	23
Initial value b_ib_j	28	1	27
Sum	120	11	109

5.3. Difference between processes with different parameter values of V_C

Three differences are extracted by comparing the transition processes of $V_C = 308.1$ and 309.75. First, a NS state exists in the transition process of $V_C = 309.75$; while no NS state exist in the transition process of $V_C = 308.1$. Second, the minimum coupling strength for CS of network with $V_C = 309.75$ ($g_c = 1.71$) is lower than that of network with $V_C = 308.1$ ($g_c = 2.19$). Third, when $V_C = 308.1$, the network is more likely to achieve the CS of period-2 bursting that corresponds to large g_c. When $V_C = 309.75$, the network is more likely to achieve CS of period-1 bursting.

5.4. Cause of the increase in the number of spikes within a burst

The increase in the maximum number of spikes within a burst with g_c increasing can be interpreted by the coupling item. For example, the number of spikes within a burst of neuron 1 when $V_C = 308.1$ and initial value a_1b_2 is shown in Fig. 17(a). Correspondingly, the maximum values (Fig. 17(b)) of the coupling item of neuron 1 increase and the minimum values (Fig. 17(c)) decrease as g_c increases. This is consistent with the fact that the stronger the stimulus (i.e., the coupling in this condition) to the neuron, the more spikes there are within the burst.

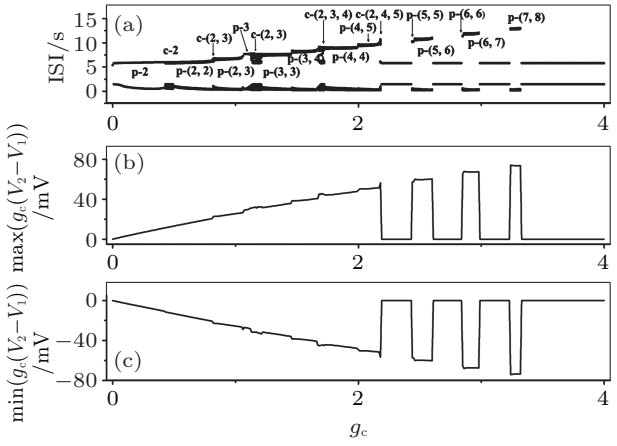


Fig. 17. (a) The transitions of neuron 1 when $V_C = 308.1$ and initial value a_1b_2; (b) maximum value of the coupling item of neuron 1; (c) minimum value of the coupling item of neuron 1. The characters "p" and "c" are abbreviations of "period" and "chaos," respectively.

6. Conclusions and discussion

Recently, the spike and burst synchronization and the transition from the burst synchronization to the spike synchronization have been widely investigated.[17–22] In this paper, the Chay model shows that period-1 bursting and period-2 bursting coexist within a parameter range, and the coexisting behavior lies between mono-stable period-1 and period-2 bursting. As V_C increases, the attraction domain of period-1 bursting increases while that of the coexisting period-2 bursting decreases. Various synchronization states, including complete synchronization, spike phase synchronization, burst phase synchronization, lag synchronization, and non-synchronization, are simulated in a network constructed by two bi-directionally coupled Chay model neurons with coexisting period-1 and period-2 bursting. The burst phase synchronization is identified as chaos synchronization and spike phase synchronization as synchronization of periodicity.

With increasing coupling strength g_c, the coupled neurons can achieve complete synchronization states via complex processes. The process depends on the parameter values within the coexisting parameter region and on the initial values. When the coexisting behavior is near period-1 bursting, the process can be divided into four parts. Part 1 is the non-synchronization. Part 2 represents the transitions between burst phase and spike phase synchronization. The processes of part 1 and part 2 are insensitive to initial values. Part 3 represents the transitions between spike phase and complete synchronization. The transit times and range of g_c depend on initial values. Part 4 represents complete synchronization. Most initial values lead to complete synchronization of period-1 bursting and fewer initial values lead to complete synchronization of period-2 bursting when g_c is large enough. When the coexisting behavior is near the period-2 bursting, three parts similar to parts 2, 3, and 4 are simulated. Most initial values lead to complete synchronization of period-2 bursting and fewer initial values lead to complete synchronization of period-1 bursting when g_c is large enough. The increase of the probability that CS of period-1 bursting will be achieve is, to a certain extent, consistent with the increase of attraction domain of period-1 bursting. The dependence of the transitions on the parameter values is consistent with the results of a previous study.[37] The synchronization transitions of this paper show more complex characteristics than those in previous works.[31–38] The most important finding of this paper is the sensitivity of the process to the initial values, especially for those transitions between spike phase and complete synchronization and for the complete synchronization. The dependence of the process on initial values was given little attention in previous works.[31–38] The synchronization processes that are complex, show a dependence on the initial values and

parameters, contain transitions between spike and burst synchronization and between phase and complete synchronization, and chaos synchronization are all helpful to understand the complex spatiotemporal behaviors of networks[45–51] and synchronization transitions in the nervous system.[31–38]

The burst synchronization was found to be a chaos synchronization. This shows that chaos synchronization can be caused by cooperation between neurons with periodic behaviors. The transition between spike and burst phase synchronization states also illustrate the transition between chaos synchronization and synchronization of periodic behaviors. When the coexisting behavior is near mono-stable period-1 bursting, we simulate the non-synchronization of bursting pattern at small coupling strength. The behavior of the non-synchronization state jumps between the coexisting attractors, which is similar to the asynchronous synchronization reported in a previous work.[31]

The number of spikes per burst of non-complete synchronous bursting increases with increasing coupling strength. This shows that bursting with multiple spikes per burst can be caused by the cooperation between neurons with one or two spikes per burst. Physiologically, bursting patterns with multiple spikes per burst can often be recorded by neurons of the central nervous system.[12–16] The results in this paper indicate that the physiologically recorded bursting with multiple spikes per burst may originate from cooperation between neurons.

From the results of the related investigations[31–38] and this paper, we conclude that the transitions from non-synchronization to complete synchronization with increasing coupling strength, which depends on parameter values and initial values, can be simulated in the coupled systems. These systems show multi-stable or coexisting behaviors when isolated. Various detailed characteristics are shown for specific networks with coexisting behaviors.[31–38] In the future, more investigations should be performed to reveal more general dynamics of network with coexisting behaviors. The structure of the attraction domain may be helpful to understand the complex transitions. In Ref. [37], the attraction domain is continuous and no chaos synchronization appears. In the present paper, the attraction domain shows a discrete structure or possible fractal structure. In addition, the transitions in Ref. [37] looks simpler than those in the present paper. Combining the trajectory of the coupled system and the attraction domain may be helpful to further identify the dynamics of the complex transitions.

References

[1] Arenas A, Díaz-Guilera A, Kurths J, Moreno Y and Zhou C S 2008 *Phys. Rep.* **469** 93
[2] Glass L 2001 *Nature* **410** 27
[3] Pecora L M and Carroll T L 1990 *Phys. Rev. Lett.* **64** 821
[4] Singer W and Gray C M 1995 *Annu. Rev. Neurosci.* **18** 555
[5] Llinás R and Ribary U 1993 *Proc. Natl. Acad. Sci. USA* **90** 2078
[6] Hartline D K 1979 *Biol. Cybern.* **33** 223
[7] Kim K H, Yoon J, Kim J H and Junq K Y 2008 *Brain Res.* **1236** 105
[8] Choi J W, Jung K Y, Kim C H and Kim K H 2010 *Neurosci. Lett.* **468** 156
[9] Bartsch R, Kantelhardt J W, Penzel T and Havlin S 2007 *Phys. Rev. Lett.* **98** 54102
[10] Buzsáki G and Draguhn A 2004 *Science* **304** 1926
[11] Gray C M, König P, Engel A K and Singer W 1989 *Nature* **338** 334
[12] Jefferys J G and Haas H L 1982 *Nature* **300** 448
[13] Kepecs A, Wang X J and Lisman J 2002 *J. Neurosci.* **22** 9053
[14] Kepecs A and Lisman J 2003 *Network* **14** 103
[15] Sun X J, Lei J Z, Perc M, Kurths J and Chen G R 2011 *Chaos* **21** 016110
[16] Ando H, Suetani H, Kurths J and Aihara K 2012 *Phys. Rev. E* **86** 016205
[17] Batista C A, Viana R L, Ferrari F A, Lopes S R, Batista A M and Coninck J C 2013 *Phys. Rev. E* **87** 042713
[18] Gu H G, Pan B B and Xu J 2014 *EPL* **106** 50003
[19] Gu H G, Li Y Y, Jia B and Chen G R 2013 *Physica A* **392** 3281
[20] Droz M and Lipowski A 2003 *Phys. Rev. E* **67** 056204
[21] Liang X, Tang M, Dhamala M and Liu Z 2009 *Phys. Rev. E* **80** 066202
[22] Wang Q Y, Chen G R and Perc M 2011 *PLoS One* **6** e15851
[23] Ozbudak E M, Thattai M, Lim H N, Shraiman B I and Van Oudenaarden A 2004 *Nature* **427** 737
[24] Guttman R, Lewis S and Rinzel J 1980 *J. Physiol.* **30** 377
[25] Izhikevich E M 2000 *Int. J. Bifurcat. Chaos* **10** 1171
[26] Tateno T and Pakdaman K 2004 *Chaos* **14** 511
[27] Lechner H A, Baxter D A, Clark J W and Byrne J H 1996 *J. Neurophysiol.* **75** 957
[28] Fröhlich F and Bazhenov M 2006 *Phys. Rev. E* **74** 031922
[29] Cymbalyuk G and Shilnikov A 2005 *J. Comput. Neurosci.* **18** 255
[30] Xu Y L, Yang M H, Liu Z Q, Liu H J, Gu H G and Ren W 2007 *Dyn. Contin. Discrete Impuls. Syst. Ser. B* **14** 35
[31] Pisarchik A N, Jaimes-Reátegui R and García-López J H 2008 *Phil. Trans. R. Soc. A* **366** 459
[32] Pisarchik A N, Jaimes-Reátegui R and García-López J H 2008 *Int. J. Bifurcat. Chaos* **18** 1801
[33] Pisarchik A N, Jaimes-Reátegui R, Villalobos-Salazar J R, García-López J H and Boccaletti S 2006 *Phys. Rev. Lett.* **96** 244102
[34] Sausedo-Solorio J M and Pisarchik A N 2011 *Phys. Lett. A* **375** 3677
[35] Ruiz-Oliveras F R and Pisarchik A N 2009 *Phys. Rev. E* **79** 016202
[36] Wang Q Y, Duan Z S, Feng Z S, Chen G R and Lu Q S 2008 *Physica A* **387** 4404
[37] Gu H G, Li Y Y, Jia B and Chen G R 2013 *Physica A* **392** 3281
[38] Bing J 2014 *Chin. Phys. B* **23** 050510
[39] Chay T R 1985 *Physica D* **16** 233
[40] Gu H G 2013 *Chaos* **23** 023126
[41] Gu H G and Xiao W W 2014 *Int. J. Bifurcat. Chaos* **24** 1450082
[42] Gu H G, Ren W, Lu Q S, Wu S G and Chen W J 2001 *Phys. Lett. A* **285** 63
[43] Hestrin S and Galarreta M 2005 *Trends Neurosci.* **28** 304
[44] Chow C and Kopell N 2000 *Neural Comput.* **12** 1643
[45] Wang H J, Huang H B and Qi G X 2005 *Phys. Rev. E* **72** 037203
[46] Pikovsky A, Zaks M, Rosenblum M, Osipov G and Kurths J 1997 *Chaos* **7** 680
[47] Chen J Y, Wong K W and Shuai J W 2002 *Phys. Rev. E* **66** 056203
[48] Taherion S and Lai Y C 1999 *Phys. Rev. E* **59** 6247
[49] Corron N J, Blakely J N and Pethel S D 2005 *Chaos* **15** 023110
[50] Wu X and Ma J 2013 *PLoS One* **8** e55403
[51] Ma J, Huang L, Wang C N and Pu Z S 2013 *Commun. Theor. Phys.* **59** 233